

Large Orbital Magnetic Moment and Strong Perpendicular Magnetic Anisotropy in Heavily Intercalated Fe_xTiS_2

Goro Shibata,^{*,†,‡} Choongjae Won,^{¶,§} Jaewook Kim,^{||} Yosuke Nonaka,[†] Keisuke Ikeda,[†] Yuxuan Wan,^{†,⊥} Masahiro Suzuki,[†] Tsuneharu Koide,[#] Arata Tanaka,[@] Sang-Wook Cheong,^{||,¶,§} and Atsushi Fujimori^{*,†,△}

[†]*Department of Physics, The University of Tokyo, Tokyo, Japan*

[‡]*Department of Applied Physics, Tokyo University of Science, Tokyo, Japan*

[¶]*Max Planck POSTECH/Korea Research Initiative, Pohang University of Science and Technology, Pohang, Korea*

[§]*Laboratory of Pohang Emergent Materials, Pohang Accelerator Laboratory, Pohang, Korea*

^{||}*Department of Physics and Astronomy, Rutgers University, Piscataway, New Jersey, USA*

[⊥]*The Institute for Solid State Physics, The University of Tokyo, Kashiwa, Japan*

[#]*Institute of Materials Structure Science, High Energy Accelerator Research Organization, Tsukuba, Ibaraki, Japan*

[@]*Department of Quantum Matter, Hiroshima University, Hiroshima, Japan*

[△]*Department of Applied Physics, Waseda University, Tokyo, Japan*

E-mail: shibata@rs.tus.ac.jp; fujimori@phys.s.u-tokyo.ac.jp

Phone: +81(3)-5876-1717

Abstract

Titanium disulfide TiS_2 , which is a member of layered transition-metal dichalcogenides with the 1T- CdI_2 -type crystal structure, is known to exhibit a wide variety of magnetism through intercalating various kinds of transition-metal atoms of different concentrations. Among them, Fe-intercalated titanium disulfide Fe_xTiS_2 is known to be ferromagnetic with strong perpendicular magnetic anisotropy (PMA) and large coercive fields (H_c). In order to study the microscopic origin of the magnetism of this compound, we have performed X-ray absorption spectroscopy (XAS) and X-ray magnetic circular dichroism (XMCD) measurements on single crystals of heavily intercalated Fe_xTiS_2 ($x \sim 0.5$). The grown single crystals showed a strong PMA with a large H_c of $\mu_0 H_c \simeq 1.0$ T. XAS and XMCD spectra showed that Fe is fully in the valence states of 2+ and that Ti is in an itinerant electronic state, indicating electron transfer from the intercalated Fe atoms to the host TiS_2 bands. The Fe^{2+} ions were shown to have a large orbital magnetic moment of $\simeq 0.59 \mu_B/\text{Fe}$, to which, combined with the spin-orbit interaction and the trigonal crystal field, we attribute the strong magnetic anisotropy of Fe_xTiS_2 .

Introduction

Ferromagnetism in systems where the distance between $3d$ transition-metal atoms is unusually long has attracted strong interest of researchers. Typical systems are diluted ferromagnetic semiconductors such as $\text{Ga}_{1-x}\text{Mn}_x\text{As}$ ¹ and double perovskites such as $\text{Sr}_2\text{FeMoO}_6$,² where hybridization between the relatively localized $3d$ orbitals of the transition-metal atoms and the itinerant, more extended orbitals plays the crucial role.

Recently, there has been keen interest in transition-metal dichalcogenides (TMDs) as a family of two-dimensional materials due to their novel physical properties.³⁻⁶ TMDs have stacked crystal structures in which two-dimensional AX_2 layers consisting of triangular lattices of the transition-metal atoms A sandwiched by the chalcogen atoms X are coupled

with each other through weak van der Waals forces. In these compounds, one can intercalate other $3d$ transition-metal atoms M into the van der Waals gaps. The intercalated compounds, M_xAX_2 , are known to exhibit a wide variety of structural, magnetic, and transport properties, including paramagnetic, ferromagnetic (FM), antiferromagnetic (AFM), and spin-glass behaviors and magneto-transport, depending on the host compound, the intercalated atom M , and its concentration x .^{7–10} Titanium disulfide TiS_2 is one of the TMDs with the 1T- CdI_2 -type layered crystal structure, where the Ti atom is surrounded by six S atoms octahedrally. Extensive studies on the structural,¹¹ transport,^{12,13} and magnetic properties^{9,10,14} of M_xTiS_2 have been made so far. Among the transition-metal intercalated titanium disulfides, the Fe-intercalated compound Fe_xTiS_2 has been found to be FM in an exceptionally wide range of Fe concentrations x ($0.2 \lesssim x \leq 1$).^{9,10,14–16} Moreover, the FM Fe_xTiS_2 has been shown to exhibit strong perpendicular magnetic anisotropy (PMA) with a large coercive field (H_c) of $\gtrsim 1$ T.^{9,10,14–16} It has also been reported that this FM state exhibits spin-glass-like behaviors, called the “cluster-glass” state, observed by ac susceptibility measurements,^{9,16} magnetotransport measurements,¹⁷ and neutron scattering.¹⁸ Effects of the ordering of the intercalated Fe atoms, observed by transmission electron microscopy,^{17,19} are also thought to be important in order to explain the x dependence of the magnetic phases.

In an attempt to understand the origin of the diverse magnetic properties of these intercalated compounds M_xTiS_2 from the viewpoint of electronic structures, first-principles calculations^{20–22} and photoemission spectroscopy^{22–28} studies have been performed so far. The importance of hybridization between the guest transition-metal atoms and the host TiS_2 has been pointed out based on the first-principles calculations.^{20–22} Magnetic coupling between the guest transition-metal atoms thus deduced is mapped onto the Ruderman-Kittel-Kasuya-Yosida (RKKY) model, and is used to explain the complex magnetic phases as a function of the concentration x .^{29,30} As for the magnetism of Fe_xTiS_2 , X-ray absorption spectroscopy (XAS) and X-ray magnetic circular dichroism (XMCD) measurements for $x = 0–0.33$ have

also been performed.²⁷ Systematic changes in the spectral line shapes as functions of x for both the Fe and the Ti absorption edges have been observed.²⁷ The presence of a large orbital magnetic moment of Fe observed by XMCD has also been pointed out.²⁷ However, the relationship between the observed large orbital magnetic moment and the strong PMA has not been discussed in sufficient detail. In addition, the magnetism of Fe_xTiS_2 at higher x 's is more interesting because it has higher FM transition temperatures and coercive fields than that at lower x 's.^{9,10} Therefore, spectroscopic studies on heavily intercalated Fe_xTiS_2 crystals have been desired.

In the present study, we have performed XAS and XMCD experiments on single crystals of heavily intercalated Fe_xTiS_2 ($x \sim 0.5$). The grown single crystals showed a strong PMA with a large H_c of $\mu_0 H_c \simeq 1.0$ T. XAS and XMCD spectra indicate electron transfer from the intercalated Fe atoms to the TiS_2 host. The Fe^{2+} ions are shown to have a large orbital magnetic moment of $\simeq 0.59 \pm 0.08 \mu_B/\text{Fe}$, which would be associated with the strong magnetic anisotropy of Fe_xTiS_2 .

Methods

Fe_xTiS_2 single crystals with $x \sim 0.5$ were grown by the typical chemical vapor deposition method. First, stoichiometric mixed powder with an I_2 transport agent in evacuated quartz tubes was heated at 500 K for 24 h to prevent the explosion of the ampule. Then, the sealed ampule was heated at 1173 K for 2 weeks with a temperature difference of 50 K between the both ends of the ampule. Detailed methods for the sample preparation are described in Ref. 31. The crystallinity of the sample was checked by X-ray diffraction (XRD) using the X'Pert Pro diffractometer from PANalytical. The conventional θ - 2θ method in the specular geometry was adopted. The X-ray source was the Cu $K\alpha$ line (wavelength $\lambda = 0.15418$ nm) and the operation voltage and current of the X-ray tube were 40 kV and 30 mA, respectively. The stoichiometry of the crystals was checked by energy dispersive X-ray (EDX)

spectroscopy equipped with a scanning electron microscope (SEM). The magnetic properties of the grown crystals were measured using the superconducting quantum interference device magnetometry.

The XAS and XMCD spectra at the Fe $L_{2,3}$ ($2p \rightarrow 3d$) and Ti $L_{2,3}$ edges were measured using a vector-magnet XMCD measurement apparatus^{32,33} installed at beamline BL-16A of Photon Factory, High Energy Accelerator Research Organization (KEK-PF). The samples were cleaved *in situ* prior to measurements. Figure 1 schematically describes the experimental geometry of the XMCD measurements. The vacuum was maintained at $\sim 1 \times 10^{-7}$ Pa during the entirety of the measurements. The samples were cooled down to $T = 30$ K without a magnetic field. The magnetic field was then applied parallel to the c -axis of the samples with the X-ray incident angle of 45° . The maximum magnetic field was 1 T. XAS signals were collected in the total electron yield mode.

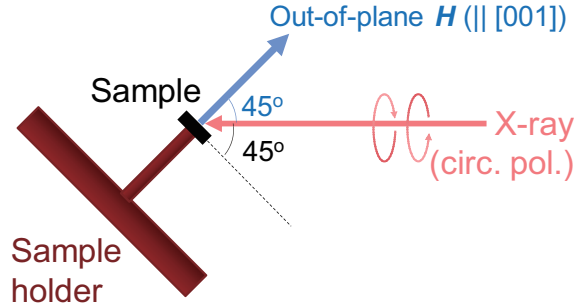


Figure 1: Experimental geometry of the X-ray magnetic circular dichroism (XMCD) measurements.

From the measured XAS and XMCD spectra, the orbital (M_{orb}) and spin (M_{spin}) magnetic moments of Fe were deduced using the XMCD sum rules.^{34,35} The explicit forms of the XMCD sum rules are given as follows.^{34,35}

$$M_{\text{orb}} = -\frac{4 \int_{L_3+L_2} (\mu_+(E) - \mu_-(E)) dE}{3 \int_{L_3+L_2} (\mu_+(E) + \mu_-(E)) dE} (10 - N_d), \quad (1)$$

$$M_{\text{spin}} = -\frac{2 \int_{L_3} (\mu_+(E) - \mu_-(E)) dE - 4 \int_{L_2} (\mu_+(E) - \mu_-(E)) dE}{\int_{L_3+L_2} (\mu_+(E) + \mu_-(E)) dE} (10 - N_d), \quad (2)$$

where $\mu_+(E)$ and $\mu_-(E)$ are the XAS spectra for the right- and left-circular polarizations, respectively, L_3 (L_2) are the absorption peaks corresponding to the Fe $2p_{3/2} \rightarrow 3d$ ($2p_{1/2} \rightarrow 3d$) transition, E is the photon energy, N_d is the number of electrons in the transition-metal $3d$ band, and M_{orb} and M_{spin} are given in the unit of measure of μ_B/atom . $N_d = 6$, which is the nominal number of electrons in an Fe^{2+} ion, was assumed in the present study. In the original references,^{34,35} the denominator is the sum of three XAS spectra, $(\mu_+(E) + \mu_-(E) + \mu_0(E))$ (where $\mu_0(E)$ is the XAS spectra for the linear polarization along the X-ray incident direction), which were approximated by $(3/2)(\mu_+(E) + \mu_-(E))$ here. In order to apply the sum rules to measured spectra, a continuum background was subtracted from the raw XAS spectra as follows: First, a polygonal line bent at the L_3 XAS peak position was subtracted so that the pre-edge and the post-edge regions became horizontal. Then, a smoothed two-step background was subtracted, which is composed of two arctangent functions with relative heights of 2 : 1 centered at the peak positions of the L_3 and L_2 edges. We note that the arbitrariness of these background subtraction procedures causes systematic errors of $\sim \pm(10\text{--}15)\%$ in the integrated XAS intensities. In Eq. (2), the spectra have been divided into the L_3 - and L_2 -edge regions at $E = 718$ eV. It is known that, when using the sum rules, the division of the XAS and XMCD spectra into the L_3 and L_2 edges at a certain energy may result in the underestimation of M_{spin} .^{36,37} The presence of an additional term called the magnetic dipole term M_T ,^{34,38,39} which has been omitted in Eq. (2), may also cause some systematic errors in M_{spin} . According to Ref. 37, the magnitude of the systematic errors of M_{spin} due to the incomplete L_3 - L_2 separation and the magnetic dipole term M_T are estimated to be about -10% and $\pm 5\%$, respectively, in the case of an Fe^{2+} ion. Hereafter, only the statistical errors of M_{orb} and M_{spin} are presented.

The spectral line shapes of the XAS and XMCD spectra were analyzed based on the configuration-interaction (CI) cluster model⁴⁰ using the XTLS 8.5 package.⁴⁰ We assumed an $[\text{FeS}_6]^{10-}$ cluster (i.e., divalent Fe) with D_{3d} symmetry, i.e., the FeS_6 octahedron is slightly elongated or shrunk along a trigonal axis. The following parameters were adjusted in order

to obtain the best-fit spectra: U_{dd} (Coulomb energy between two Fe $3d$ valence electrons), U_{dc} (Coulomb energy between the Fe $3d$ electron and the Fe $2p$ core electron), Δ (charge-transfer energy), $(pd\sigma)$ (Slater-Koster parameters), $10Dq$ (octahedral crystal field), D_{trg} (trigonal crystal field), and H_{mol} (molecular field). Spin-orbit interaction (SOI) and the Slater integrals were estimated from atomic Hartree-Fock calculations. For the Slater integrals, 80% of the values deduced from the atomic Hartree-Fock calculation were used. In the CI calculation, the ground state was assumed to be a linear combination of the $3d^6$, $3d^7\bar{L}$, and $3d^8\bar{L}^2$ configurations, where \bar{L} is a ligand hole.

Results and Discussion

Sample Characterization

Figure 2 shows the XRD profile of an Fe_xTiS_2 ($x \sim 0.5$) single crystal. Sharp Bragg peaks along the $[001]$ direction are clearly observed, confirming the layered structure of the grown crystal. From the obtained XRD profile, the out-of-plane lattice parameter c has been estimated to be 0.572 nm, close to the value $c = 0.574$ nm obtained in the previous study for Fe_xTiS_2 with $x = 0.5$.¹¹

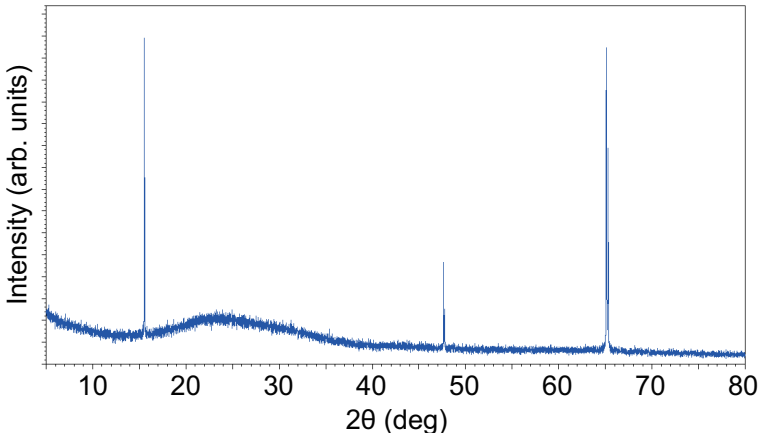


Figure 2: X-ray diffraction (XRD) profile along the out-of-plane $[001]$ direction of an Fe_xTiS_2 ($x \sim 0.5$) single crystal.

Figure 3(a) shows the SEM image of the Fe_xTiS_2 single crystal on a carbon tape. The

typical sample diameter is 0.5–1 mm. Regions with flat surfaces can be seen with typical sizes of a few hundred micrometers squared. The EDX spectrum of the crystal is shown in Fig. 3(b). From the spectral intensities, the atomic ratio of each element has been estimated to be Fe : Ti : S = 12.7 : 28.5 : 58.8, which corresponds to the chemical formula $\text{Fe}_{0.432}\text{Ti}_{0.968}\text{S}_2$. This confirms that more Fe atoms are intercalated in the present Fe_xTiS_2 crystal than those in the previous XMCD study ($x \leq 0.33$),²⁷ although the Fe concentration is slightly lower than the nominal value ($x = 0.5$).

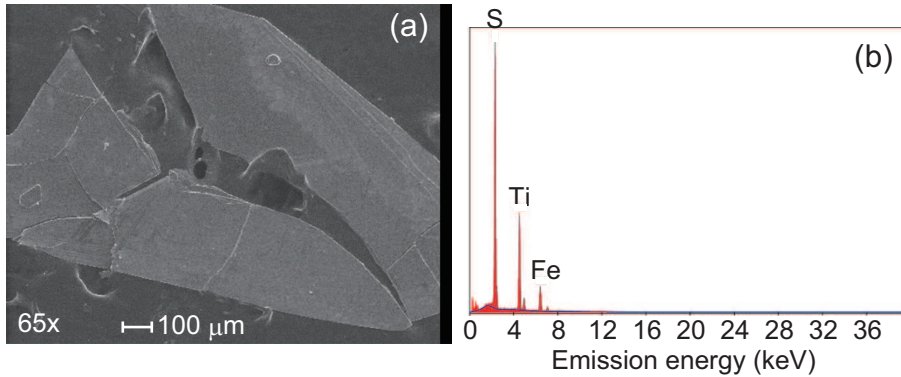


Figure 3: Energy dispersive X-ray spectroscopy (EDX) analysis of an Fe_xTiS_2 single crystal. (a) Scanning electron microscope (SEM) image of the Fe_xTiS_2 single crystal on a carbon tape. (b) EDX spectrum.

From the temperature dependence of the magnetization, the Curie temperature of the crystal has been estimated to be ~ 70 K. Figure 4 shows the zero-field cooled (ZFC) magnetization curve of the Fe_xTiS_2 ($x \sim 0.5$) single crystal measured at 2 K with an applied magnetic field \mathbf{H} parallel to the c -axis (trigonal axis) up to $\mu_0|\mathbf{H}| = 7$ T. In the initial magnetization process, a sudden jump in the magnetization M is observed around $\mu_0 H \sim 1$ T, suggesting a transition from the AFM to FM states. After magnetic saturation, a clear rectangular hysteresis loop is observed with a coercive field H_c of $\mu_0 H_c \sim 1$ T. The obtained H_c is similar to those of polycrystalline Fe_xTiS_2 with ($x = 0.33$ – 0.45) and single-crystalline $\text{Fe}_{0.33}\text{TiS}_2$ reported in the previous study.¹⁰ The large hysteresis loop suggests that the crystal exhibits a strong PMA with the magnetic easy axis along the c -axis. We note that quantitative estimate of the saturation magnetization M_{sat} from the raw magnetization curve

is difficult due to a large uncertainty of the sample mass. We have, therefore, plotted the magnetization curve normalized by M_{sat} in Fig. 4. We shall deduce the values of M_{sat} and the uniaxial magnetic anisotropy energy (MAE) K_{u} by the XMCD measurements afterward.

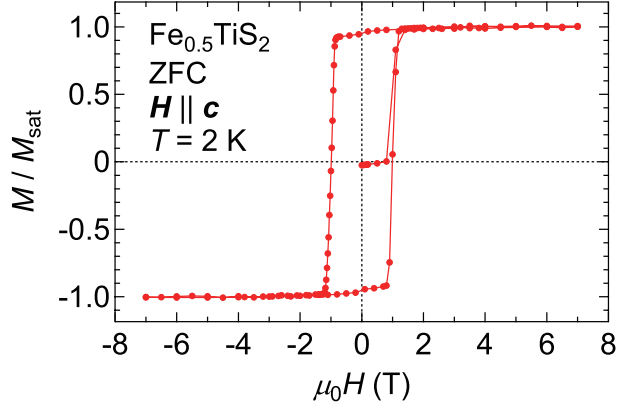


Figure 4: Normalized magnetization curve of the $\text{Fe}_{0.5}\text{TiS}_2$ single crystal.

X-ray Magnetic Circular Dichroism Spectroscopy

Figure 5(a) shows the helicity-averaged XAS spectra of the Fe_xTiS_2 ($x \sim 0.5$) single crystal at the Fe $L_{2,3}$ ($2p_{1/2,3/2} \rightarrow 3d$) absorption edges. The XAS spectra of divalent and trivalent iron oxides and metallic iron are also shown as references.^{41,42} The overall spectral line shape of $\text{Fe}_{0.5}\text{TiS}_2$ is similar to that of FeO. Especially, the small shoulder around $h\nu = 706.5$ eV is characteristic of divalent Fe, showing that the iron atom is essentially in the Fe^{2+} valence state. Reflecting the large hybridization strength of sulfides and high electrical conductivity compared to oxides, the XAS spectrum of $\text{Fe}_{0.5}\text{TiS}_2$ shows broader absorption peaks and more extended high-energy tails than that of FeO. One may think that the XAS spectrum of $\text{Fe}_{0.5}\text{TiS}_2$ is also similar to that of the Fe metal. As indicated in Fig. 5(a) by arrows, however, the XAS spectra of $\text{Fe}_{0.5}\text{TiS}_2$ and FeO have several multiplet structures in common, while they are absent in the XAS spectrum of metallic Fe reflecting its itinerant electronic structures. This indicates that the amount of possible metallic iron clusters, if any, is small in the present $\text{Fe}_{0.5}\text{TiS}_2$ crystal. The difference of the peak positions of the multiplet structures between $\text{Fe}_{0.5}\text{TiS}_2$ and FeO is probably due to the different hybridization strength

and crystal-field splitting between oxides and sulfides.

In Fig. 5(b), the helicity-averaged XAS spectra of the Fe_xTiS_2 ($x \sim 0.5$) single crystal at the Ti $L_{2,3}$ absorption edges are compared with those of Fe_xTiS_2 ($0 \leq x \leq 0.33$)^{27,43} and titanium oxides.⁴⁴ The spectral line shape of the present $\text{Fe}_{0.5}\text{TiS}_2$ crystal is close to those of Fe_xTiS_2 with $x \leq 0.33$.²⁷ One can see that, as x increases, the absorption peaks become broader and the energy splitting between the two principal peaks in each of the L_3 and L_2 edges become systematically smaller. The shoulder structures around $h\nu = 457$ and 463 eV in the present XAS spectra are more diffuse than those for $x = 0.33$, confirming that a larger amount of Fe atoms are intercalated in the present sample than in the previous ones. These spectral changes with increasing x are considered to be due to electron doping from the intercalated Fe atoms into the TiS_2 host. As can be seen from the figure, the spectral line shapes of Fe_xTiS_2 with $x \neq 0$ cannot be described as a superposition of the Ti^{4+} and Ti^{3+} valence states. This implies that the electrons doped from Fe into TiS_2 do not lead to a mixed-valence state consisting of the Ti^{4+} and Ti^{3+} ionic states, but have rather itinerant character.

Figures 5(c)–5(f) show the helicity-dependent XAS spectra and the XMCD spectra at the Fe $L_{2,3}$ and Ti $L_{2,3}$ edges. The XMCD spectra in Figs. 5(e) and 5(f) clearly show that not only Fe but also Ti exhibits finite XMCD signals. This suggests that the observed ferromagnetism is not due to magnetic impurities such as metallic iron or iron compounds but due to the intrinsic properties of the $\text{Fe}_{0.5}\text{TiS}_2$ crystal. First-principle calculations^{20,21} show that the band structure of the transition-metal-intercalated TiS_2 is significantly modified from that of the nonintercalated TiS_2 through hybridization between the intercalated atoms and the host compound. In the case of Fe intercalation, the down-spin Fe $3d$ states hybridize with the Ti $3d$ states to form spin-polarized bands near the Fermi level.²⁰ As a result, Ti exhibits small but finite spin polarization.²⁰ The present XMCD result is qualitatively consistent with this calculation.

Using the XMCD sum rules,^{34,35} we have deduced the spin (M_{spin}) and orbital magnetic

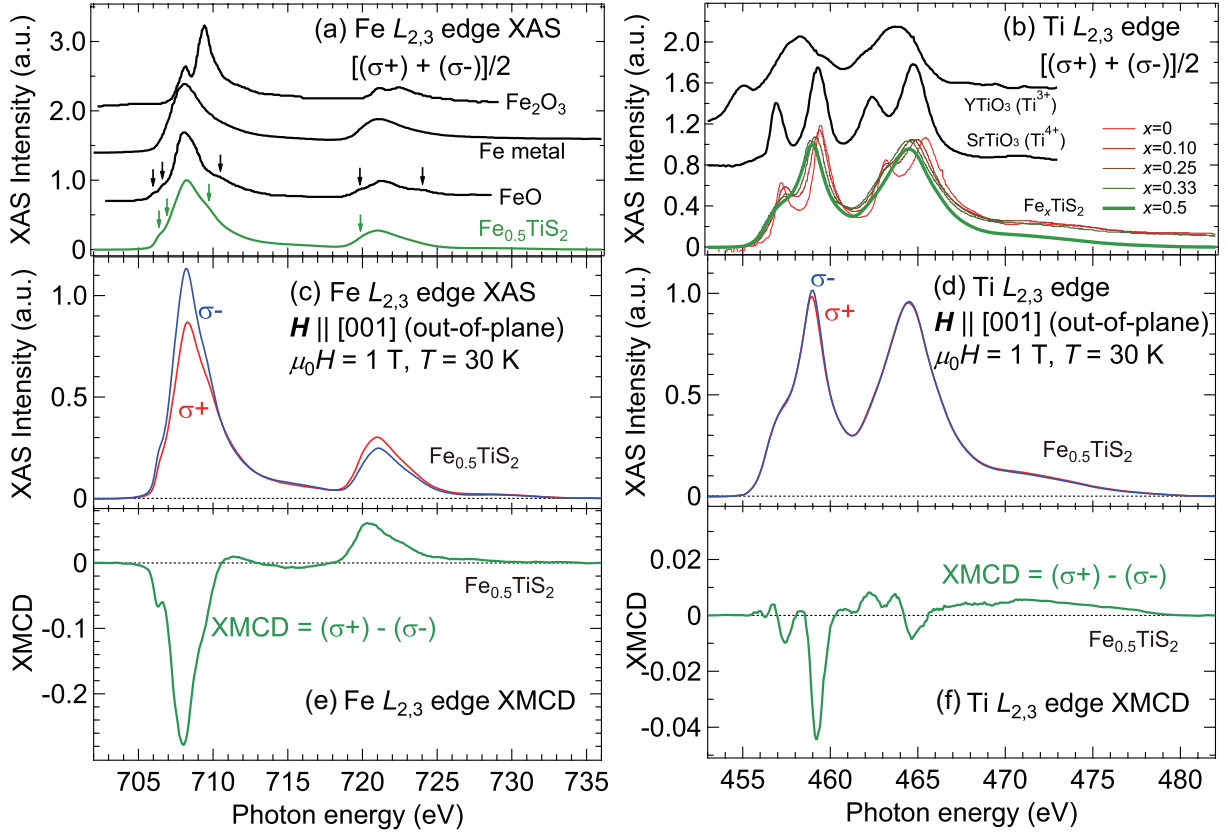


Figure 5: X-ray absorption spectroscopy (XAS) and XMCD spectra. (a,b) Helicity-averaged XAS spectrum of $\text{Fe}_{0.5}\text{TiS}_2$ at the Fe $L_{2,3}$ ($2p_{1/2,3/2} \rightarrow 3d$) (a) and Ti $L_{2,3}$ (b) absorption edges. The reference XAS spectra of iron oxides, metallic iron, and titanium oxides are taken from Refs. 41, 42, and 44, respectively. The Ti XAS spectra of TiS_2 and Fe_xTiS_2 ($0 \leq x \leq 0.33$) are taken from Refs. 43 and 27, respectively. Arrows in Panel (a) indicate the multiplet structures of Fe^{2+} , which are absent in the metallic Fe. (c,d) Helicity-dependent XAS spectra of the $\text{Fe}_{0.5}\text{TiS}_2$ single crystal at the Fe $L_{2,3}$ (c) and Ti $L_{2,3}$ (d) edges. (e,f) XMCD spectra at the Fe $L_{2,3}$ (e) and Ti $L_{2,3}$ (f) edges. The spectra were measured at the temperature (T) of 30 K under the magnetic field ($\mu_0 H$) of 1 T applied parallel to the c -axis ([001] axis). The spectra have been normalized so that the peak height of the helicity-averaged XAS spectra at the L_3 edge is equal to unity. In Panels (a)–(d), two-step backgrounds has been subtracted from the raw XAS spectra.

moments (M_{orb}) of Fe. We note that the M_{spin} of Ti cannot be deduced from the spin sum rule due to the too small spin-orbit splitting of the Ti $2p$ core levels, making the decomposition of the XMCD spectrum into the L_2 and L_3 components **impossible**.^{34,36,37} We also note that the M_{orb} of Ti, which is obtained by integrating the entire XMCD spectrum, was below the detection limit ($\sim 0.1 \mu_B/\text{atom}$) of the present experiment. Considering that the magnetization is 45° off from the X-ray incident direction, the obtained magnetic moments have been divided by $\cos 45^\circ = 1/\sqrt{2}$ in order to correct this effect. As shown in Fig. 6, the integral of the Fe XMCD spectrum has a large negative end value, suggesting that Fe has a large M_{orb} parallel to the spin magnetic moment. The results of the sum rule yield $M_{\text{spin}} = 2.45 \pm 0.16 \mu_B/\text{Fe}$ and $M_{\text{orb}} = 0.59 \pm 0.08 \mu_B/\text{Fe}$. The obtained M_{spin} is consistent with the values deduced from the first-principle calculations: $M_{\text{spin}} = 2.45 \mu_B/\text{Fe}$ for $x = 1/3$ and $M_{\text{spin}} = 2.99 \mu_B/\text{Fe}$ for $x = 1$.²⁰ The large M_{orb} may be due to the degeneracy of the electron orbitals in the Fe^{2+} valence state and the partially filled t_{2g} level in a relatively weak crystal fields for the intercalated Fe atoms.

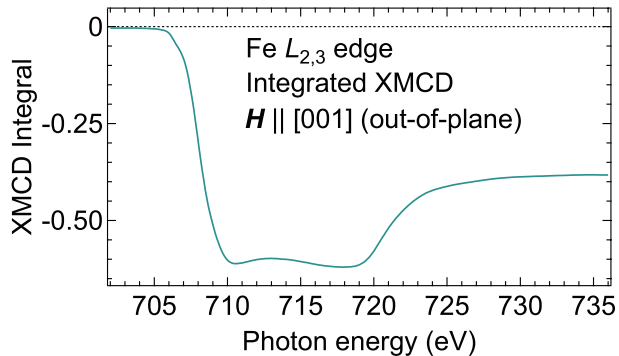


Figure 6: Integrated XMCD spectra of the $\text{Fe}_{0.5}\text{TiS}_2$ single crystal at the Fe $L_{2,3}$ edge.

From the M_{spin} and M_{orb} values deduced by using the XMCD sum rule, one can deduce the uniaxial magnetic anisotropy energy K_u based on the Stoner-Wohlfarth model,⁴⁵ in which one assumes uniaxial magnetic anisotropy and the coherent rotation of the magnetic domain. According to the model, the coercive field H_c is equal to $2K_u/(\mu_0 M_{\text{sat}})$, where $M_{\text{sat}} = 3.04 \pm 0.18 \mu_B/\text{Fe}$ is the saturation magnetization calculated as the sum of M_{spin} and M_{orb} . From this relationship, the uniaxial MAE for the present Fe_xTiS_2 single crystal

is estimated to be $K_u = 0.176 \pm 0.011$ meV/Fe or $K_u = 0.244 \pm 0.015$ MJ/m³ (note that K_u is defined positive for materials with PMA).

CI Cluster-Model Calculation

In order to explain the observed large M_{orb} of Fe and the strong PMA of $\mu_0 H_c \simeq 1.0$ T and $K_u = 0.244$ MJ/m³, we calculated the XAS and XMCD spectra at the Fe $L_{2,3}$ edges using the CI cluster model. An $[\text{FeS}_6]^{-10}$ cluster with weak trigonal distortion (D_{3d} symmetry) was employed. In the present calculation, we first optimized the parameters Δ , U_{dd} , U_{dc} , ($pd\sigma$), and $10Dq$ in the O_h symmetry (i.e., $D_{\text{trg}} = 0$) so that the calculated spectra well reproduce the experimental ones (for the definitions of $10Dq$ and D_{trg} , see the inset of Fig. 7(b)). The best-fit result was obtained with the parameter values listed in Table 1. The obtained parameter values are comparable to those deduced from the photoemission spectroscopy of $\text{Fe}_{0.33}\text{TiS}_2$.⁴⁶ We then optimized the values of H_{mol} and D_{trg} so that they reproduce the experimental M_{spin} and K_u , respectively. K_u has been calculated as the total energy difference between two spin configurations, $\mathbf{M}_{\text{spin}} \parallel [001]$ and $\mathbf{M}_{\text{spin}} \parallel [110]$. Figure 7(a) shows the H_{mol} dependence of the calculated spin magnetic moment M_{spin} . We note that modifying the values of H_{mol} only resulted in the change in the XMCD intensity, without any variation in the characteristic spectral line shapes (not shown here). By comparing the calculated M_{spin} with the experimental value, H_{mol} has been estimated to be 5 ± 1 meV. Figure 7(b) shows the D_{trg} dependence of the calculated magnetic anisotropy energy K_u . It can be seen that the experimental K_u can be reproduced by only a slight change in D_{trg} of ~ 1 meV. The calculated Fe $L_{2,3}$ XAS and XMCD spectra are shown in Figs. 7(c) and 7(d) for $D_{\text{trg}} = 0$ meV and $D_{\text{trg}} = \pm 1$ meV. The calculated spectra well reproduce the experimental spectral features. It can also be seen that the spectral line shapes and the XMCD intensities are nearly insensitive to D_{trg} , although such a small magnitude of D_{trg} can induce appreciable magnetic anisotropy as shown below.

Table 1: Best-fit parameters for the configuration-interaction (CI) cluster-model calculations.

Δ	U_{dd}	U_{dc}	$(pd\sigma)$	$10Dq$
2.5 eV	5.0 eV	6.3 eV	-0.8 eV	0.7 eV

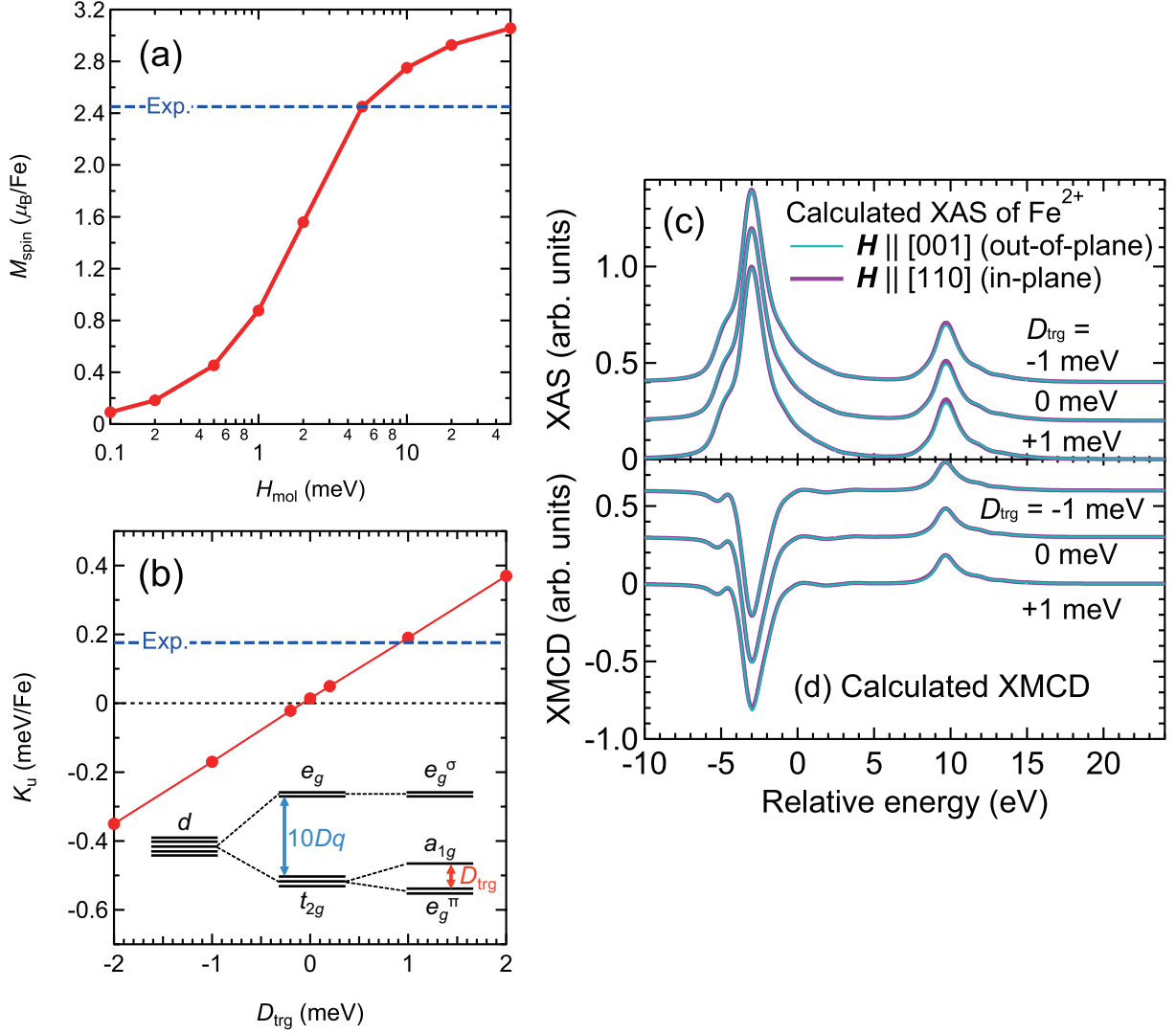


Figure 7: Results of CI cluster-model calculations at the Fe $L_{2,3}$ edge. (a) Molecular field (H_{mol}) dependence of the spin magnetic moment per Fe atom (M_{spin}). (b) Trigonal crystal field (D_{trg}) dependence of the magnetic anisotropy energy per Fe atom (K_u). In panels (a) and (b), blue dashed lines represent the experimental values. Inset of panel (b) depicts the crystal-field splitting in the case of $D_{\text{trg}} > 0$. (c),(d) Calculated XAS (c) and XMCD (d) spectra for $D_{\text{trg}} = 0$ meV and $D_{\text{trg}} = \pm 1$ meV. See Table 1 for the other parameter values used.

Discussion: Origin of the Strong PMA

The microscopic origin of the strong PMA of Fe-intercalated TMDs is discussed by Parkin and Friend⁷ based on the atomic multiplet model in an octahedral crystal field with a trigonal distortion. Here, we summarize their discussion and apply it to the present system. An Fe²⁺ ion with 3d⁶ electron configuration octahedrally coordinated by six anions has the ⁵T_{2g} ground state, which is triply degenerate in the orbital part ((t_{2g})⁴(e_g)²) and quintuply degenerate in the spin part (S = 2). (Note that the multielectron state ⁵T_{2g} should be distinguished from the one-electron state t_{2g}.) The orbital triplet is isomorphic to the substates of orbital angular momentum L = 1. In order to represent this orbital triplet, an effective orbital angular momentum operator **L**^{eff} is introduced. Using **L**^{eff}, the Hamiltonian of the system can be written as follows:

$$\hat{H} = -D_{\text{trg}}(L_z^{\text{eff}})^2 - \lambda \mathbf{L}^{\text{eff}} \cdot \mathbf{S} + \mathbf{S} \cdot \mathbf{H}_{\text{mol}}, \quad (3)$$

where the first, second, and third terms represent the energies of the trigonal crystal field D_{trg} (> 0), SOI of the 3d electrons λ (> 0), and the Zeeman effect by the molecular field \mathbf{H}_{mol} (in the unit of measure of eV) originating from exchange interactions, respectively. Note that we have replaced the Zeeman term due to the external magnetic field $\mu_B(-\mathbf{L}^{\text{eff}} + 2\mathbf{S}) \cdot \mu_0 \mathbf{H}$, which is originally introduced by Parkin and Friend,⁷ by that due to the molecular field because we consider the FM state instead of the paramagnetic one. They have treated the first two terms as the primary terms and the Zeeman term as perturbation and have shown that the energy corrections for the out-of-plane and in-plane magnetic fields are of the first and second orders in H_{mol} , respectively, resulting in the anisotropy of the g -factor. However, our cluster-model calculation shows that λ ($\simeq 50$ meV) > H_{mol} ($\simeq 5$ meV) > D_{trg} ($\simeq 1$ meV). We, therefore, treat the role of D_{trg} as perturbation to SOI and H_{mol} in order to explain the magnetic anisotropy of FM Fe_xTiS₂.

Figure 8(a) schematically describes the energy diagram of an Fe²⁺ ion based on this

model. The ${}^5T_{2g}$ ground state under the octahedral crystal field is split into three levels of $J^{\text{eff}} = 1, 2, 3$ by SOI, where $\mathbf{J}^{\text{eff}} = \mathbf{L}^{\text{eff}} + \mathbf{S}$ is the effective total angular momentum. Since λ is 1 order of magnitude larger than the thermal energy $k_B T$ (~ 2.5 meV), only the $J^{\text{eff}} = 1$ level has to be considered. The $J^{\text{eff}} = 1$ level is then Zeeman-split into three sublevels of $m = 1, 0, -1$, where m is the magnetic quantum number for \mathbf{J}^{eff} . The magnetic anisotropy energy can be deduced by calculating the difference of the perturbation energy of D_{trg} in the cases of out-of-plane ($\mathbf{H}_{\text{mol}} \parallel \mathbf{z}$) and in-plane molecular fields ($\mathbf{H}_{\text{mol}} \parallel \mathbf{x}$). The ground state $|J^{\text{eff}} = 1, m = 1\rangle$ is expressed as follows in the cases of ($\mathbf{H}_{\text{mol}} \parallel \mathbf{z}$) and ($\mathbf{H}_{\text{mol}} \parallel \mathbf{x}$):

$$\begin{aligned}
|J^{\text{eff}} = 1, m = 1\rangle_z &= |J^{\text{eff}} = 1, J_z^{\text{eff}} = 1\rangle \quad (\mathbf{H}_{\text{mol}} \parallel \mathbf{z}), \\
|J^{\text{eff}} = 1, m = 1\rangle_x &= \frac{1}{2}|J^{\text{eff}} = 1, J_z^{\text{eff}} = 1\rangle \\
&\quad + \frac{1}{\sqrt{2}}|J^{\text{eff}} = 1, J_z^{\text{eff}} = 0\rangle \\
&\quad + \frac{1}{2}|J^{\text{eff}} = 1, J_z^{\text{eff}} = -1\rangle \quad (\mathbf{H}_{\text{mol}} \parallel \mathbf{x}),
\end{aligned}$$

where the $|J^{\text{eff}} = 1, J_z^{\text{eff}}\rangle$ terms can be written using the eigenstates of L_z^{eff} and S_z (denoted as $|L_z, S_z\rangle$) as

$$\begin{aligned}
|J^{\text{eff}} = 1, J_z^{\text{eff}} = 1\rangle &= \sqrt{\frac{6}{10}}|-1, 2\rangle - \sqrt{\frac{3}{10}}|0, 1\rangle + \sqrt{\frac{1}{10}}|1, 0\rangle, \\
|J^{\text{eff}} = 1, J_z^{\text{eff}} = 0\rangle &= \sqrt{\frac{3}{10}}|-1, 1\rangle - \frac{2}{\sqrt{10}}|0, 0\rangle + \sqrt{\frac{3}{10}}|1, -1\rangle, \\
|J^{\text{eff}} = 1, J_z^{\text{eff}} = -1\rangle &= \sqrt{\frac{1}{10}}|-1, 0\rangle - \sqrt{\frac{3}{10}}|0, -1\rangle + \sqrt{\frac{6}{10}}|1, -2\rangle,
\end{aligned}$$

Thus, the perturbation energies due to the trigonal crystal field $\langle -D_{\text{trg}} (L_z^{\text{eff}})^2 \rangle$ for the out-of-plane and in-plane fields can be calculated as $-D_{\text{trg}}/4$ and $-D_{\text{trg}}/16$, respectively, to the first order of D_{trg} . This energy shift is schematically described in Fig. 8(b). This energy difference can be regarded as the origin of the PMA in the present system. We stress that this is a first-order perturbation effect, which is the reason why such a small magnitude of

D_{trg} can give rise to the considerable magnitude of the magnetic anisotropy energy. The present result is consistent with the D_{trg} dependence of K_u shown in Fig. 7(b), in which K_u is nearly proportional to D_{trg} when the crystal field is weak.

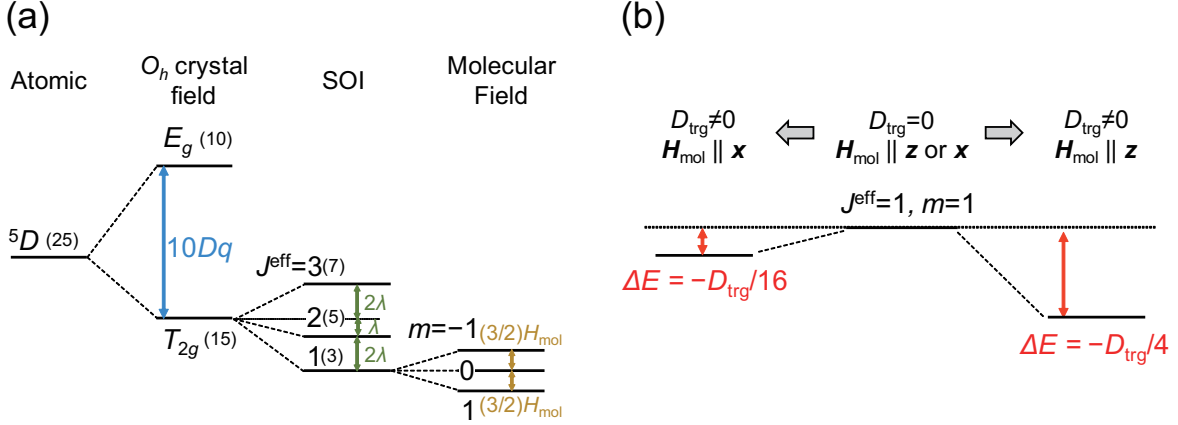


Figure 8: Schematic energy diagram of the Fe^{2+} ion ($3d^6$ electron configuration) octahedrally coordinated by six anions with small trigonal distortion. (a) Energy splitting due to the octahedral crystal field ($10Dq$), SOI (λ), and molecular field (H_{mol}). The numbers in parentheses denote the degeneracy. (b) Energy shift due to the trigonal crystal field D_{trg} in the cases of out-of-plane ($\mathbf{H}_{\text{mol}} \parallel \mathbf{z}$) and in-plane molecular fields ($\mathbf{H}_{\text{mol}} \parallel \mathbf{x}$).

The present XMCD results show that there exists a large unquenched orbital moment of the intercalated Fe atom ($\simeq 0.59\mu_B/\text{Fe}$) in $\text{Fe}_{0.5}\text{TiS}_2$, which is considered to originate from the above-mentioned effective orbital angular momentum in the $5T_{2g}$ state. The ratio of the orbital to spin angular momentum ($\langle L_z \rangle / \langle S_z \rangle = 2M_{\text{orb}} / M_{\text{spin}}$) is calculated to be 0.48 ± 0.07 . According to the previous XMCD measurements for Fe_xTiS_2 with $x \leq 0.33$,²⁷ the values of $\langle L_z \rangle / \langle S_z \rangle$ are deduced to be 0.49, 0.48, and 0.25 for $x = 0.10$, 0.25, and 0.33, respectively. The $\langle L_z \rangle / \langle S_z \rangle$ value obtained for $x = 0.5$ in the present study is out of this decreasing tendency with increasing x . Although the mechanism for this x dependence of $\langle L_z \rangle / \langle S_z \rangle$ is not clear at present, hybridization effects between guest Fe and host TiS_2 , which have not been taken into account in the above discussion, might be relevant. We note that similar x dependence has also been observed in the strength of the coercive field H_c of Fe_xTiS_2 .^{9,10} We expect that the complex x dependence of H_c can be explained by the magnitude of the unquenched orbital magnetic moment of the intercalated Fe^{2+} ions.

Conclusion

We have performed XAS and XMCD experiments on single crystals of heavily intercalated Fe_xTiS_2 ($x \sim 0.5$) in order to discuss the microscopic origin of the strong PMA and large H_c of this compound. We have confirmed that the grown single crystal showed a large H_c of $\mu_0 H_c \simeq 1.0$ T and strong PMA with a magnetic anisotropy energy K_u of 0.244 MJ/m³. From the XMCD result, the Fe^{2+} ions are shown to have a large orbital magnetic moment of $\simeq 0.59 \pm 0.08 \mu_B/\text{Fe}$. The strong magnetic anisotropy of Fe_xTiS_2 is attributed to the large orbital moment combined with the spin-orbit interaction and the trigonal crystal field.

Acknowledgement

A.F. and S.W.C. would like to thank D. D. Sarma for long-standing collaboration on a variety of interesting $3d$ transition-metal compounds and for stimulating interaction during the last many decades. We thank Kenta Amemiya and Masako Sakamaki for valuable technical support at KEK-PF. This work was supported by Grants-in-Aid for Scientific Research from the JSPS (15H02109, 15K17696, 19K03741, and 20K14416). J.W.K. and S.W.C. were supported by the National Science Foundation (NSF) under Grant No. DMR-1629059. C.J.W. and S.W.C. partially were supported by the National Research Foundation of Korea (NRF) funded by the Ministry of Science and ICT(No. 2016K1A4A4A01922028 and No. 2020M3H4A2084417). Y.X.W. acknowledges support from Advanced Leading Graduate Course for Photon Science (ALPS) at the University of Tokyo. A.F. is an adjunct member of Center for Spintronics Research Network (CSRN), the University of Tokyo, under Spintronics Research Network of Japan (Spin-RNJ). The experiment was done under the approval of the Photon Factory Program Advisory Committee (Proposal No. 2016S2-005, No. 2016G066, and No. 2019G622).

The authors declare no competing financial interest.

References

- (1) Mahadevan, P.; Zunger, A.; Sarma, D. D. Unusual directional dependence of exchange energies in GaAs diluted with Mn: Is the RKKY description relevant? Phys. Rev. Lett. **2004**, 93, 177201.
- (2) Sarma, D. D.; Mahadevan, P.; Saha-Dasgupta, T.; Ray, S.; Kumar, A. Electronic structure of $\text{Sr}_2\text{FeMoO}_6$. Phys. Rev. Lett. **2000**, 85, 2549–2552.
- (3) Lee, J. Y.; Shin, J. H.; Lee, G. H.; Lee, C. H. Two-dimensional semiconductor optoelectronics based on van der Waals heterostructures. Nanomaterials (Basel) **2016**, 6, 193.
- (4) Choi, W.; Choudhary, N.; Han, G. H.; Park, J.; Akinwande, D.; Lee, Y. H. Recent development of two-dimensional transition metal dichalcogenides and their applications. Mater. Today **2017**, 20, 116–130.
- (5) Manzeli, S.; Ovchinnikov, D.; Pasquier, D.; Yazyev, O.; Kis, A. 2D transition metal dichalcogenides. Nat. Rev. Mater. **2017**, 2, 17033.
- (6) Pal, B.; Singh, A.; G., S.; Mahale, P.; Kumar, A.; Thirupathaiah, S.; Sezen, H.; Amati, M.; Gregoratti, L.; Waghmare, U. V. et al. Chemically exfoliated MoS_2 layers: Spectroscopic evidence for the semiconducting nature of the dominant trigonal metastable phase. Phys. Rev. B **2017**, 96, 195426.
- (7) Parkin, S. S. P.; Friend, R. H. 3d transition-metal intercalates of the niobium and tantalum dichalcogenides. I. Magnetic properties. Philos. Mag. B **1980**, 41, 65–93.
- (8) Parkin, S. S. P.; Friend, R. H. 3d transition-metal intercalates of the niobium and tantalum dichalcogenides. II. Transport properties. Philos. Mag. B **1980**, 41, 95–112.
- (9) Inoue, M.; Matsumoto, M.; Negishi, H.; Sakai, H. Low field ac magnetic susceptibility

- measurements of intercalation compounds $M_x\text{TiS}_2$ ($M=3d$ transition metals). J. Magn. Magn. Mater. **1985**, 53, 131–138.
- (10) Negishi, H.; Shoube, A.; Takahashi, H.; Ueda, Y.; Sasaki, M.; Inoue, M. Magnetic properties of intercalation compounds $M_x\text{TiS}_2$ ($M = 3d$ transition metal). J. Magn. Magn. Mater. **1987**, 67, 179–186.
- (11) Inoue, M.; Negishi, H. Interlayer spacing of 3d transition-metal intercalates of 1T-CdI₂-type TiS_2 . J. Phys. Chem. **1986**, 90, 235–238.
- (12) Koyano, M.; Negishi, H.; Ueda, Y.; Sasaki, M.; Inoue, M. Electrical resistivity and thermoelectric power of intercalation compounds $M_x\text{TiS}_2$ ($M=\text{Mn, Fe, Co, and Ni}$). Phys. Status Solidi B **1986**, 138, 357–363.
- (13) Inoue, M.; Koyano, M.; Negishi, H.; Ueda, Y. Electronic properties of intercalation compound Fe_xTiS_2 . J. Phys. Soc. Jpn. **1986**, 55, 1400–1401.
- (14) Negishi, H.; Koyano, M.; Inoue, M.; Sakakibara, T.; Goto, T. High field magnetization of 3d transition metal intercalates $M_x\text{TiS}_2$ ($M=3d$ metals). J. Magn. Magn. Mater. **1988**, 74, 27–30.
- (15) Yoshioka, T.; Tazuke, Y. Magnetic properties of Fe_xTiS_2 system. J. Phys. Soc. Jpn. **1985**, 54, 2088–2091.
- (16) Negishi, H.; Ōhara, S.; Koyano, M.; Inoue, M.; Sakakibara, T.; Goto, T. Anisotropic spin-glass and cluster-glass of layered Fe_xTiS_2 crystals. J. Phys. Soc. Jpn. **1988**, 57, 4083–4085.
- (17) Choe, J.; Lee, K.; Huang, C.-L.; Trivedi, N.; Morosan, E. Magnetotransport in Fe-intercalated TS_2 : Comparison between $T = \text{Ti}$ and Ta. Phys. Rev. B **2019**, 99, 064420.
- (18) Kuroiwa, Y.; Honda, H.; Noda, Y. Neutron magnetic scattering of intercalation compounds Fe_xTiS_2 . Mol. Cryst. Liq. Cryst. Sci. Technol., Sect. A **2000**, 341, 15–20.

- (19) Chiew, Y. L.; Miyata, M.; Koyano, M.; Oshima, Y. Ordering of intercalated Fe atoms in Fe_xTiS_2 structures clarified using transmission electron microscopy. J. Phys. Soc. Jpn. **2020**, 89, 074601.
- (20) Suzuki, N.; Yamasaki, T.; Motizuki, K. Electronic band structures of intercalation compounds of 3d transition metals with TiS_2 . J. Magn. Magn. Mater. **1987**, 70, 64–66.
- (21) Suzuki, N.; Yamasaki, T.; Motizuki, K. Electronic band structures and bond orders of $\text{M}_{1/3}\text{TiS}_2$ (M=Mn, Fe, Co, Ni). J. Phys. Soc. Jpn. **1989**, 58, 3280–3289.
- (22) Martinez, H.; Tison, Y.; Baraille, I.; Loudet, M.; Gonbeau, D. Experimental (XPS/STM) and theoretical (FLAPW) studies of model systems $\text{M}_{1/4}\text{TiS}_2$ (M=Fe, Co, Ni): influence of the inserted metal. J. Electron. Spectrosc. Relat. Phenom. **2002**, 125, 181–196.
- (23) Ueda, Y.; Negishi, H.; Koyano, M.; Inoue, M.; Soda, K.; Sakamoto, H.; Suga, S. Resonant photoemission studies of 3d transition metal intercalates of TiS_2 . Solid State Commun. **1986**, 57, 839–842.
- (24) Ueda, Y.; Fukushima, K.; Negishi, H.; Inoue, M.; Taniguchi, M.; Suga, S. Photoemission studies on intercalation compounds of M_xTiS_2 (M=3d transition metals). J. Phys. Soc. Jpn. **1987**, 56, 2471–2476.
- (25) Fujimori, A.; Suga, S.; Negishi, H.; Inoue, M. X-ray photoemission and Auger-electron spectroscopic study of the electronic structure of intercalation compounds M_xTiS_2 (M=Mn, Fe, Co, and Ni). Phys. Rev. B **1988**, 38, 3676–3689.
- (26) Suga, S. Angle-resolved, resonance-and inverse-photoemission studies of transition metal intercalated TiS_2 . Mol. Cryst. Liq. Cryst. Sci. Technol., Sect. A **2000**, 341, 9–14.
- (27) Yamasaki, A.; Imada, S.; Sekiyama, A.; Suga, S.; Matsushita, T.; Muro, T.; Saitoh, Y.;

- Negishi, H.; Sasaki, M. Angle-resolved photoemission spectroscopy and magnetic circular dichroism in Fe-intercalated TiS_2 . Surf. Rev. Lett. **2002**, 9, 961–966.
- (28) Suga, S.; Tusche, C.; ichiro Matsushita, Y.; Ellguth, M.; Irizawa, A.; Kirschner, J. Momentum microscopy of the layered semiconductor TiS_2 and Ni intercalated $\text{Ni}_{1/3}\text{TiS}_2$. New J. Phys. **2015**, 17, 083010.
- (29) Tazuke, Y.; Ohta, Y.; Miyamoto, S. Exchange interactions in Fe_xTiS_2 . J. Phys. Soc. Jpn. **2005**, 74, 2644–2645.
- (30) Tazuke, Y.; Miyashita, T.; Nakano, H.; Sasaki, R. Magnetic properties of M_xTiSe_2 ($\text{M}=\text{Mn}, \text{Fe}, \text{Co}$). Phys. Status Solidi C **2006**, 3, 2787–2790.
- (31) Lévy, F., Ed. Intercalated Layered Materials; D. Reidel Publishing Company: Dordrecht, Holland, 1979.
- (32) Furuse, M.; Okano, M.; Fuchino, S.; Uchida, A.; Fujihira, J.; Fujihira, S.; Kadono, T.; Fujimori, A.; Koide, T. HTS vector magnet for magnetic circular dichroism measurement. IEEE Trans. Appl. Supercond. **2013**, 23, 4100704.
- (33) Shibata, G.; Kitamura, M.; Minohara, M.; Yoshimatsu, K.; Kadono, T.; Ishigami, K.; Harano, T.; Takahashi, Y.; Sakamoto, S.; Nonaka, Y. et al. Anisotropic spin-density distribution and magnetic anisotropy of strained $\text{La}_{1-x}\text{Sr}_x\text{MnO}_3$ thin films: angle-dependent x-ray magnetic circular dichroism. npj Quantum Mater. **2018**, 3, 3.
- (34) Carra, P.; Thole, B. T.; Altarelli, M.; Wang, X. X-ray circular dichroism and local magnetic fields. Phys. Rev. Lett. **1993**, 70, 694–697.
- (35) Thole, B. T.; Carra, P.; Sette, F.; van der Laan, G. X-ray circular dichroism as a probe of orbital magnetization. Phys. Rev. Lett. **1992**, 68, 1943–1946.
- (36) Teramura, Y.; Tanaka, A.; Jo, T. Effect of Coulomb interaction on the x-ray magnetic

- circular dichroism spin sum rule in $3d$ transition elements. J. Phys. Soc. Jpn. **1996**, 65, 1053–1055.
- (37) Piamonteze, C.; Miedema, P.; de Groot, F. M. F. Accuracy of the spin sum rule in XMCD for the transition-metal L edges from manganese to copper. Phys. Rev. B **2009**, 80, 184410.
- (38) Stöhr, J.; König, H. Determination of spin- and orbital-moment anisotropies in transition metals by angle-dependent x-ray magnetic circular dichroism. Phys. Rev. Lett. **1995**, 75, 3748–3751.
- (39) Dürr, H. A.; van der Laan, G. Magnetic circular x-ray dichroism in transverse geometry: Importance of noncollinear ground state moments. Phys. Rev. B **1996**, 54, R760–R763.
- (40) Tanaka, A.; Jo, T. Resonant $3d$, $3p$ and $3s$ photoemission in transition metal oxides predicted at $2p$ threshold. J. Phys. Soc. Jpn. **1994**, 63, 2788–2807.
- (41) Regan, T. J.; Ohldag, H.; Stamm, C.; Nolting, F.; Lüning, J.; Stöhr, J.; White, R. L. Chemical effects at metal/oxide interfaces studied by x-ray-absorption spectroscopy. Phys. Rev. B **2001**, 64, 214422.
- (42) Chen, C. T.; Idzerda, Y. U.; Lin, H.-J.; Smith, N. V.; Meigs, G.; Chaban, E.; Ho, G. H.; Pellegrin, E.; Sette, F. Experimental confirmation of the x-ray magnetic circular dichroism sum rules for iron and cobalt. Phys. Rev. Lett. **1995**, 75, 152–155.
- (43) Kimura, A.; Suga, S.; Matsushita, T.; Imada, S.; Shino, N.; Saitoh, Y.; Shigeoka, H.; Daimon, H.; Kinoshita, T.; Kakizaki, A. et al. Electronic structure of Ni intercalated TiS_2 probed by angle resolved and $2p$ core resonance photoemission as well as by $2p$ core absorption spectroscopy. Jpn. J. Appl. Phys. **1993**, 32, 255–257.
- (44) Cao, Y.; Liu, X.; Kareev, M.; Choudhury, D.; Middey, S.; Meyers, D.; Kim, J.-

- W.; Ryan, P.; Freeland, J.; Chakhalian, J. Engineered Mott ground state in a $\text{LaTiO}_{3+\delta}/\text{LaNiO}_3$ heterostructure. Nat. Commun. **2016**, 7, 10418.
- (45) Stoner, E. C.; Wohlfarth, E. P. A mechanism of magnetic hysteresis in heterogeneous alloys. Philos. Trans. R. Soc., A **1948**, 240, 599–642.
- (46) Bocquet, A. E.; Mizokawa, T.; Saitoh, T.; Namatame, H.; Fujimori, A. Electronic structure of $3d$ -transition-metal compounds by analysis of the $2p$ core-level photoemission spectra. Phys. Rev. B **1992**, 46, 3771–3784.